Received December 6, 2019, accepted December 18, 2019, date of publication January 3, 2020, date of current version January 17, 2020.

*Digital Object Identifier 10.1109/ACCESS.2019.2963693*

# Fault Estimation and Fault Tolerant Control Strategies Applied to VTOL Aerial Vehicles With Soft and Aggressive Actuator Faults

**GERARDO ORTIZ-TORRES[1], PEDRO CASTILLO[2], FELIPE D. J. SORCIA-VÁZQUEZ[1], JESSE Y. RUMBO-MORALES[1], JORGE A. BRIZUELA-MENDOZA[1], JAVIER DE LA CRUZ-SOTO[3], AND MARIO MARTÍNEZ-GARCÍA[1]**

[1]Computer Science and Engineering Department, University of Guadalajara, Ameca 46600, Mexico
[2]Sorbonne Universités, Université de Technologie de Compiègne, CNRS, Heudiasyc 7253, 60200 Compiègne, France
[3]National Institute for Electricity and Clean Energy, Cuernavaca 62490, Mexico

Corresponding author: Felipe D. J. Sorcia-Vázquez (felipe.sorcia@valles.udg.mx)

This work was supported in part by the Consejo Nacional de Ciencia y Tecnología (CONACyT), Mexico, and in part by the French Government Research Programm Investissements d'avenir through the Robotex Equipment of Excellence under Grant ANR-10-EQPX-44.

**ABSTRACT** Actuator Fault Estimation (FE) and Fault Tolerant Control (FTC) strategies designed with model-based observers for Vertical Take-Off and Landing (VTOL) aerial vehicles are proposed and validated experimentally in this paper. Three observers are considered for FE: a nonlinear adaptive observer and a linear Proportional-Integral Observer (PIO) applied to a Planar VTOL and a quasi-Linear Parameter Varying (qLPV) PIO applied to a quadcopter vehicle. The fault detection is done by comparing the fault estimation signal with a predefined threshold. Fault isolation is achieved by analyzing the sign of the fault estimation signal. The Available Control Authority Index (ACAI) method is used to analyze the controllability properties of the vehicles under actuator faults. The main contribution of this work is the design and the experimental validation of complete active FTC schemes by using the proposed FE systems in order to accommodate a soft actuator fault and reconfigure an aggressive fault, even when the vehicle is flying in a non-hover position. Finally, the proposed FTC schemes are validated in different cases of flight tests for illustrating the effectiveness of the strategies.

**INDEX TERMS** Fault tolerant control, fault diagnosis, actuators, safely, aircraft, controllability, propellers.

## I. INTRODUCTION

In the last years multicopter configurations for Unmanned Aerial Vehicles (UAVs) have become promising mobile platforms capable of navigating (semi) autonomously in uncertain environments. Numerous applications for this kind of vehicles have been proposed, as aerial photography, surveillance, crop spraying, oil spill detection, supply delivery, fire monitoring, agriculture assessment, communications monitoring, among others [1]. Among them, the VTOLs (Vertical Take-Off and Landing) vehicles have proved to be suitable for these applications due to the fact that they can take-off and landing in reduced spaces and they are essentially simpler to build compared with conventional helicopters [2]. The most popular VTOL vehicles are PVTOL (Planar VTOL) and the quadcopter.

The associate editor coordinating the review of this manuscript and approving it for publication was Gursel Alici.

With the increase of applications and the high degree of integrating automation technology, the VTOL aircraft have become progressively vulnerable to faults which inevitably influence the dynamics of the vehicle affecting the stability, reliability, and safety during the flight envelope. In order to identify malfunctions at any time and to improve reliability and safety in the VTOL, Fault Tolerant Control (FTC) methods can be considered. The FTC techniques are classified into two types [3]: passive and active. In the active techniques the controller parameters are adapted or reconfigured according to the fault using the information of the Fault Diagnosis (FD) system, so that the stability and acceptable performance of the system can be holded. Observers have been extensively used for FD schemes. Recently, [4], [5] have proposed a robust fault reconstruction using two sliding mode observers in cascade. Simulation example demonstrates the efficacy of the proposed schemes. Some works have considered actuator FD for quadcopters: in [6], an experimental applications

have showed a fast actuator fault isolation and estimation using a Two-Stage Kalman Filter (TSKF). In [7] and [8], the FD was performed using polynomial and Thau observers, respectively. The previous works consider that the actuator fault occur when the vehicle is flying in a hover position. This means that the vehicle is flying in a stationary position without nonlinear dynamics presented.

Recent works on active FTC design for quadcopter vehicles subjected to actuator partial faults can be found in [9]–[14]. In [12], [13] the faults were injected when the vehicle is flying at hover position. To the best of our knowledge, the only experimental validation for a quadcopter flying in a non-hover position is presented in [14]. The authors have developed a FD and accommodation algorithm using nonlinear adaptive estimation techniques. Adaptive thresholds were designed to detect and isolate actuator faults. In [15]–[21] aggressive actuator faults or failures have been considered in the design of the FTC systems. Only [19] presents a complete active FTC scheme with the design of a FD system. Rotational dynamics of the quadcopter vehicle is used in order to estimate the failure. The simulation results show that the fault is correctly detected and a safe flight can be maintained even after the complete loss of one rotor. The remaining works consider that the fault detection, isolation and estimation tasks are already accomplished. In [22] FE and FTC strategy based on a Nonlinear Unknown Input Observer (NUIO) is applied to a fixed PVTOL system with both actuator drift and oscillation faults and saturation. Simulation results have shown the effectiveness of the proposed methodology.

Usually the mathematical model of a VTOL is represented by a set of ordinary differential equations [23]–[25] or linear approximations [26]. However an alternative to represent its nonlinear dynamics is through a collection of linear subsystems. Recently, Linear Parameter Varying (LPV) systems have garnered much interest [27]. An accurate representation of the nonlinear system can be obtained by considering the sector-nonlinearity approach, also known as quasi-LPV (qLPV) because the scheduling functions are represented by nonlinear state or input dependent functions. According to the literature, there are relatively few studies on designing FTC and FD methods based on qLPV systems applied to a VTOL aircraft. For example, robust passive, active and hybrid actuator fault tolerant LPV controllers for rotational dynamics are given in [28]. The comparison illustrates that the hybrid FTC method reduces the effect that the fault estimation error has on the closed-loop response. The limitation in [28] is that the number of local models grows exponentially with respect to the number of faults taken into consideration. Moreover, the FD problem is not considered. The only experimental results (from our best knowledge) using this technique and reported in the literature is presented in [13]. However, its drawback comes from the LPV representation, that it is based on a very simplified linear model, and the actuator faults (considered as time-varying parameters) are injected when the quadcopter is flying at hover position. In [29] an integrated active LPV FTC scheme using sliding modes is presented. The gain in the LPV observer and the static feedback LPV controller are synthesized simultaneously to optimize the performance of the closed-loop system. Even the works reported in the literature, the design and experimental validation of FD systems using the LPV representation of a VTOL aircraft remains important and a challenging problem to be solved in a theoretical and practical way.

In order to design an effective FTC strategy it is necessary to determine how the faults affect the vehicle by analyzing the controllability and the performance degradation of the system due to the faults. However, classical controllability theories are not sufficient to test the controllability of a VTOL aircraft because the actuators only provide unidirectional lift. To analyze how the actuators faults affect the vehicle, in [30] the construction of an Available Control Authority Index (ACAI) is proposed to quantify the control authority of the vehicle as a function of the available actuators and their physical limits. Recently, [31] developed an attitude controllability analysis for a multicopter in case of several actuators failures by using the Small Time Local Controllability (STLC) of the system. These works concluded that it is necessary to test the static controllability of a VTOL aircraft before any FTC strategies are employed. However, no controllability test was applied to a quadcopter vehicle to analyze how different type of actuator faults affect its performance.

This paper presents FD systems designed with three Fault Estimation (FE) observers for VTOL vehicles: a nonlinear Adaptive Observer (AO) and a linear Proportional-Integral Observer (PIO) both applied to a PVTOL aircraft, and finally a qLPV PIO applied to a quadcopter vehicle. The main contribution of this work is the design and the experimental validation of a complete active FTC schemes by using the FE systems in order to accommodate a soft actuator fault and reconfigure an aggressive fault presented in a VTOL aircraft, even when the vehicle is flying in a non-hover position. The design of the FTC schemes procedure can be explained as follows: 1) an analysis of controllability of the VTOL systems (PVTOL and quadcopter) is applied using the ACAI method in order to test the performance degradation of the vehicle under soft and aggressive actuator faults; 2) a nonlinear AO, linear PIO and qLPV PIO are applied for performing actuator fault estimation. The fault detection is done by comparing the fault estimation signal with a predefined threshold. Fault isolation is achieved by analyzing the sign of the fault estimation signal. Sufficient conditions for the existence of the PI observers is given in terms of Linear Matrix Inequalities (LMIs); 3) a nominal PD controller is considered to track the 3D position and attitude dynamics of the VTOL ensuring a desired performance in a fault-free case; 4) finally, the Fault Accommodation (FA) or Fault Reconfiguration (FR) control law is achieved using the nominal controller and the FD system for retaining close to nominal fault-free performance despite partial actuator fault. The proposed active FTC schemes are validated in different cases of flight tests for illustrating the fesibility and effectiveness of the FD systems.

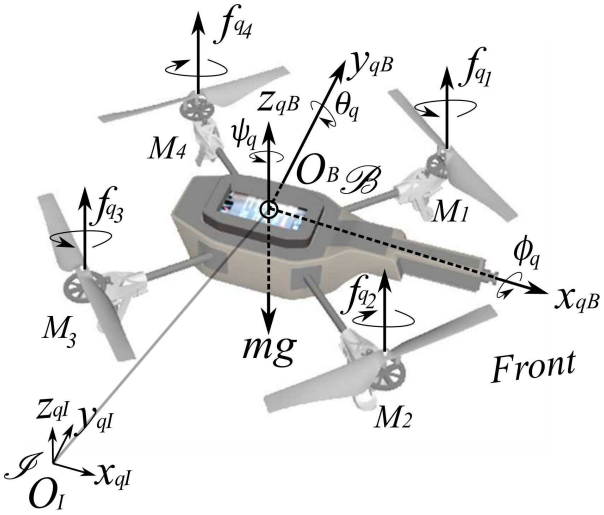


**FIGURE 1.** Quadcopter scheme representing main forces acting in the vehicle.

The remainder of this paper is arranged as follows. The VTOL dynamics equations are presented in Section II. Section III states the problem formulation and the main goal of this paper. In Section IV, the fault estimation systems are designed. The active FTC schemes are developed in Section V. In Section VI, the proposed schemes are validated experimentally in flight tests, main graphs illustrating the system performance are depicted. Discussion about our results are presented in Section VII.

## II. PRELIMINARIES

The studied VTOL system is the well known quadcopter aerial vehicle shown in Fig. 1, whose parameters are given in Table 1.

The quadcopter vehicle is composed of four independent motors with four propellers that produce torques and thrusts in the direction of the propeller axis of rotation, as depicted in Fig. 1. From this figure, $\mathcal{I}$ denotes an inertial frame, and $\mathcal{B}$ represents a rigid frame attached to the Center of Mass (CoM) of the vehicle.

By using the Newton-Euler formalism, the dynamics for a quadcopter vehicle can be expressed as

$$\begin{cases} \ddot{\phi}_q(t) = \dot{\theta}_q(t)\dot{\psi}_q(t)\left(\frac{J_y - J_z}{J_x}\right) \\ -\frac{J_{rz}}{J_x}\dot{\theta}_q(t)\Omega_M(t) + \frac{l}{J_x}u_{q_2}(t), \\ \ddot{\theta}_q(t) = \dot{\phi}_q(t)\dot{\psi}_q(t)\left(\frac{J_z - J_x}{J_y}\right) \\ +\frac{J_{rz}}{J_y}\dot{\phi}_q(t)\Omega_M(t) + \frac{l}{J_y}u_{q_3}(t), \\ \ddot{\psi}_q(t) = \dot{\phi}_q(t)\dot{\theta}_q(t)\left(\frac{J_x - J_y}{J_z}\right) + \frac{d}{J_z}u_{q_4}(t), \end{cases} \tag{1a}$$

$$\left\{\ddot{z}_q(t) = -g + c\theta_q(t)c\phi_q(t)\frac{1}{m}u_{q_1}(t), \right. \tag{1b}$$

$$\begin{cases} \ddot{x}_q(t) = \big(c\psi_q(t)s\theta_q(t)c\phi_q(t) \\ +s\psi_q(t)s\phi_q(t)\big)\frac{1}{m}u_{q_1}(t), \\ \ddot{y}_q(t) = \big(s\psi_q(t)s\theta_q(t)c\phi_q(t) \\ -c\psi_q(t)s\phi_q(t)\big)\frac{1}{m}u_{q_1}(t), \end{cases} \tag{1c}$$

**TABLE 1.** Parameters of the quadcopter vehicle.

| Parameter | Value | Unit |
|---|---|---|
| Mass of the vehicle, $m$ | 0.4080 | Kg |
| Acceleration due to gravity, $g$ | 9.8066 | m/s$^2$ |
| Aerodynamic coefficient, $d$ | 0.0301 | N·m/N |
| Distance between a rotor and CoM, $l$ | 0.1785 | m |
| Moment of inertia about $x_q$ and $x_p$, $J_x$ | 0.0022 | Kg·m$^2$ |
| Moment of inertia about $y_q$, $J_y$ | 0.0029 | Kg·m$^2$ |
| Moment of inertia about $z_q$, $J_z$ | 0.0048 | Kg·m$^2$ |
| Motor's maximum thrust force, $f_{v_{max}}$ | 1.93 | N |
| Propeller's moment of inertia about $z_q$, $J_{rz}$ | $2.029 \times 10^{-5}$ | Kg·m$^2$ |

where $\xi(t) = [x_q(t), y_q(t), z_q(t)]^\top \in \mathbb{R}^3$ denotes the position of the vehicle with respect to the frame $\mathcal{I}$, $t$ is the time variable, $\Omega(t) = [\dot{\phi}_q(t), \dot{\theta}_q(t), \dot{\psi}_q(t)]^\top \in \mathbb{R}^3$ represents the angular velocity of the aircraft defined in $\mathcal{B}$, $c$ and $s$ indicate the trigonometric functions cos and sin, respectively. The overall residual propeller angular speed is $\Omega_M(t)$ and $d$ denotes an aerodynamic coefficient that characterizes the relation between the reaction torque and thrust force. The system inputs for the attitude dynamics (1a) are defined as $\mathbf{u}_r(t) = [u_{q_2}(t), u_{q_3}(t), u_{q_4}(t)]^\top$ while the control input for the altitude (1b) and translational displacements (1c) is $u_{q_1}(t)$. However the real inputs of system (1) are the upward lifting forces. Then, the following relation can be stated

$$\mathbf{u}_q(t) = \begin{bmatrix} \frac{u_{q_1}(t)}{\mathbf{u}_r(t)} \end{bmatrix} = \underbrace{\left[\begin{array}{cccc} 1 & 1 & 1 & 1 \\ \hline 1 & -1 & -1 & 1 \\ 1 & 1 & -1 & -1 \\ -1 & 1 & -1 & 1 \end{array}\right]}_{\Delta_q} \underbrace{\begin{bmatrix} f_{q_1}(t) \\ f_{q_2}(t) \\ f_{q_3}(t) \\ f_{q_4}(t) \end{bmatrix}}_{\bar{f}_q(t)} \tag{2}$$

When the quadcopter vehicle is evolving in its longitudinal (or lateral) plane, it can be considered as a PVTOL aircraft. In this aircraft, yaw dynamics is not considered, and therefore left actuators can be used to generate a force $f_{p_1}(t) = f_{q_1}(t) + f_{q_4}(t)$, and similarly right actuators can produce the force $f_{p_2}(t) = f_{q_2}(t) + f_{q_3}(t)$. Hence, from (1), the following nonlinear model for the PVTOL can be obtained

$$\ddot{\phi}_p(t) = \frac{l}{J_x}u_{p_2}(t), \tag{3a}$$

$$\ddot{z}_p(t) = -g + c\phi_p(t)\frac{1}{m}u_{p_1}(t), \tag{3b}$$

$$\ddot{y}_p(t) = -s\phi_p(t)\frac{1}{m}u_{p_1}(t), \tag{3c}$$

by assuming that the remaining states are already stabilized.

For the PVTOL vehicle, we can define the input vector $\mathbf{u}_p(t) = [u_{p_1}(t), u_{p_2}(t)]^\top$ as

$$\mathbf{u}_p(t) = \begin{bmatrix} u_{p_1}(t) \\ u_{p_2}(t) \end{bmatrix} = \underbrace{\begin{bmatrix} 1 & 1 \\ 1 & -1 \end{bmatrix}}_{\Delta_p} \underbrace{\begin{bmatrix} f_{p_1}(t) \\ f_{p_2}(t) \end{bmatrix}}_{\bar{f}_p(t)}. \tag{4}$$

## III. PROBLEM FORMULATION

In practice, actuator faults can be caused by damage in the propeller or the motor itself, both cases will produce a loss in the motors effectiveness. Also, a voltage variation in battery

could be seen as a motors Loss of Effectiveness (LoE), which is reasonable due to the fact that the thrust is related with the voltage of battery. Consider the presence of a multiplicative fault signal defined by

$$\mathbf{u}_{\vartheta f}(t) = \Delta_{\vartheta}\left(I_w - \bar{\lambda}_{\vartheta}(t)\right)\bar{f}_{\vartheta}(t), \tag{5}$$

where $\mathbf{u}_{\vartheta f}(t)$ represents the real faulty input applied to the VTOL system, with $\vartheta = q$ or $p$ for the quadcopter or PVTOL, respectively, $I_w$ is an identity matrix, $w$ introduces the number of actuators, $\bar{\lambda}_{\vartheta}(t) = \text{diag}\left(\lambda_{\vartheta_1}(t), \lambda_{\vartheta_2}(t), \ldots, \lambda_{\vartheta_w}(t)\right)$, where $0 \leq \lambda_{\vartheta_v}(t) \leq 1$, with $v = 1, \ldots, w$, and the value of $\lambda_{\vartheta_v}(t)$ indicates:

$$\begin{aligned}
&\lambda_{\vartheta_v}(t) = 1 && \Rightarrow \text{a total fault of the } v\text{–th actuator,}\\
&\lambda_{\vartheta_v}(t) = 0 && \Rightarrow \text{the } v\text{–th actuator is healthy,}\\
&\lambda_{\vartheta_v}(t) = ]0, 1[ && \Rightarrow \text{LoE of } v\text{–th actuator.}
\end{aligned}$$

From (2) and (4) the thrust force vector is defined as $\bar{f}_{\vartheta}(t) = [f_{\vartheta_1}(t), f_{\vartheta_2}(t), \ldots, f_{\vartheta_w}(t)]^{\top}$, where $f_{q_v}(t) \in [0, f_{v_{max}}]$ and $f_{p_v}(t) \in [0, 2f_{v_{max}}]$. Now, it is possible to rewrite (5) as an external additive fault signal

$$\mathbf{u}_{\vartheta f}(t) = \mathbf{u}_{\vartheta}(t) + \bar{\eta}_{\vartheta}(t), \tag{6}$$

where

$$\bar{\eta}_{\vartheta}(t) = -\Delta_{\vartheta}\bar{\lambda}_{\vartheta}(t)\bar{f}_{\vartheta}(t) \tag{7}$$

means the actuator fault vector affecting the VTOL system.

*Remark 1:* Subscript $\vartheta = q$ represents the overall quadcopter system (1), with the number of actuators $w = 4$ while the rotational dynamics (1a) is represented with subscript $r$. The PVTOL system (3) is indicated with subscript $\vartheta = p$, with $w = 2$.

*Assumption 1:* For easily in the practical validation, it is assumed that only one partial actuator fault (LoE) is presented in the system.

In order to analyze the controllability of the quadcopter vehicle subjected to LoE, a linear dynamic model around hover condition for attitude (1a) and altitude (1b) dynamics is written as follows

$$\dot{\mathbf{x}}_c(t) = A_c\mathbf{x}_c(t) + B_c\mathbf{u}_c(t), \tag{8}$$

with

$$A_c = \begin{bmatrix} 0_{4\times4} & I_4 \\ 0_{4\times4} & 0_{4\times4} \end{bmatrix}, \quad B_c = \begin{bmatrix} 0_{4\times4} \\ J_c \end{bmatrix},$$

$\mathbf{u}_c(t) = \mathbf{u}_{qf}(t) - G_c$, $\mathbf{x}_c(t) = [z_q(t), \phi_q(t), \theta_q(t), \psi_q(t), \dot{z}_q(t), \dot{\phi}_q(t), \dot{\theta}_q(t), \dot{\psi}_q(t)]^{\top}$, $J_c = \text{diag}(1/m, l/J_x, l/J_y, d/J_z)$, $G_c = [mg, 0, 0, 0]^{\top}$ and $\mathbf{u}_{qf}(t)$ expressed as a multiplicative actuator fault (5). From (2) and (8), $\mathbf{u}_{qf}(t)$ and $\mathbf{u}_c(t)$ are constrained by

$$\begin{aligned}
\mathcal{M} &= \{\mathbf{u}_{qf}(t) | \mathbf{u}_{qf}(t) = \Delta_q\left(I_w - \bar{\lambda}_q(t)\right)\bar{f}_q(t), \bar{f}_q(t) \in \mathcal{F}\},\\
\mathcal{U} &= \{\mathbf{u}_c(t) | \mathbf{u}_c(t) = \mathbf{u}_{qf}(t) - G_c \in \mathcal{M}\}.
\end{aligned} \tag{9}$$

The ACAI based controllability analysis method is applied to the quadcopter system (8) with the control constraints (9). Then, the following theorem can be used.

**TABLE 2. VTOL controllability analysis.**

| Fault | LoE[1] | Quadcopter and PVTOL | | Quadcopter | |
|---|---|---|---|---|---|
| | | ACAI[1] | CY[1] | ACAI-WY[1] | CY |
| Soft | 0.1 | 1.47 | CN[1] | - | - |
| | 0.2 | 1.08 | CN | - | - |
| | 0.3 | 0.70 | CN | - | - |
| | 0.4 | 0.31 | CN | - | - |
| Aggressive | 0.5 | -0.06 | UCN[1] | 1.99 | CN |
| | 0.6 | -0.45 | UCN | 1.26 | CN |
| | 0.7 | -0.84 | UCN | 0.72 | CN |
| | 0.8 | -1.22 | UCN | 0.44 | CN |
| | 0.9 | -1.61 | UCN | 0.17 | CN |

[1] LoE: Loss of effectiveness in $\lambda_{\vartheta_v}$ or $\{\lambda_{p_1}, \lambda_{p_2}\}$, CY: Controllability, ACAI: Available control authority index, ACAI-WY: ACAI without yaw, CN: Controllable, UCN: Uncontrollable.

*Theorem 1 [30]: System* (8) *is controllable, if only if the following two conditions holds: 1) Rank of* $[B_c, A_cB_c, \ldots, A_c^7B_c] = 8$*; 2) The ACAI* $\rho(G_c, \partial\mathcal{U}) > 0$*, where* $\rho(G_c, \partial\mathcal{U}) \triangleq min\{||G_c - \mathbf{u}_{qf}(t)||, \mathbf{u}_{qf}(t) \in \partial\mathcal{U}\}$ *represents the distance from* $G_c$ *to the boundary of* $\mathcal{U}$*. In other words,* $\rho(G_c, \partial\mathcal{U})$ *is the maximum control forces that can be produced in all directions.*

*Proof:* The proof and computation of $\rho(G_c, \partial\mathcal{U})$ can be consulted in [30]. □

Table 2 presents the ACAI controllability method applied to VTOL systems using parameters in Table 1. Faults are classified as soft $\lambda_{\vartheta_v} \in [0.1, 0.4]$ and aggressives $\lambda_{\vartheta_v} \in [0.5, 0.9]$. Table 2 also shown that both aircrafts are uncontrollable with an aggressive fault. It is clear that is impossible to reconfigure an aggressive fault presented in a PVTOL system because from configuration it consider only two forces. Nevertheless, analyzing the quadcopter system subjected to an aggressive fault, it can be noticed that losing controllability of yaw dynamics is a solution in order to safely recover the vehicle [15], [18]–[21]. This strategy implies to give up controlling the yaw angle, and use the remaining forces to achieve a constant horizontal spin.

Our goal is to design and validate experimentally model-based observers to estimate or at least detect and isolate the actuator LoE presented in Table 2. These observers are designed to be used in FTC schemes for fast fault detection, isolation, accommodation and reconfiguration tasks, even when the aircrafts are flying in a non-hover position.

## IV. FAULT ESTIMATION DESIGN

To reach the previous goal, we introduce in the following the design of three different observers: 1) a nonlinear AO and 2) a linear PIO both applied to the PVTOL aircraft and 3) a qLPV PIO for the quadcopter vehicle.

It is considered that the PVTOL aircraft is flying near to hover position, this implies that the nonlinearities become small. In the quadcopter vehicle the tests will be done flying at hover and non-hover position. Thus, the nonlinearities have to be considered in the fault estimation observer design. In order to address these nonlinearities, qLPV theory is applied only to the quadcopter vehicle, as an alternative for the representation of nonlinear systems.

*Assumption 2:* The fault signal is assumed to be constant over the time or at least slowly varying, such that $\dot{\bar{\eta}}_\vartheta(t) = 0$.

### A. FE USING NONLINEAR AO FOR THE PVTOL AIRCRAFT

Following some ideas from [32], the following observers have been designed. Let consider the roll and altitude dynamics of the PVTOL model (3) with actuator faults as an external additive signal (6) and no unmeasurable states. The subsystems (3a) and (3b) can be rewritten in the "nonlinear adaptive observer form" by defining the state vector as $\mathbf{x}_p(t) = [\mathbf{x}_{p_1}(t), \mathbf{x}_{p_2}(t), \mathbf{x}_{p_3}(t), \mathbf{x}_{p_4}(t)]^\top = [z_p(t), \phi_p(t), \dot{z}_p(t), \dot{\phi}_p(t)]^\top$, the faulty state vector as $\mathbf{x}_{pf}(t)$ and the actuator fault vector as $\bar{\eta}_p(t) = [\eta_{p_1}(t), \eta_{p_2}(t)]^\top$, with no unmeasurable faulty states i.e., $\mathbf{y}_{pf}(t) = \mathbf{x}_{pf}(t)$. Then, the rotational dynamics (3a) can be expressed as

$$\dot{\mathbf{x}}_{\phi f}(t) = \alpha_1 + \beta_1 \eta_{p_2}(t), \tag{10}$$

with $\mathbf{x}_{\phi f}(t) = [\mathbf{x}_{pf_2}(t), \mathbf{x}_{pf_4}(t)]^\top$,

$$\alpha_1 = \begin{bmatrix} \mathbf{x}_{pf_4}(t) \\ l u_{p_2}(t)/J_x \end{bmatrix}, \quad \beta_1 = \begin{bmatrix} 0 \\ l/J_x \end{bmatrix},$$

and the attitude dynamics (3b) as follows

$$\dot{\mathbf{x}}_{zf}(t) = \alpha_2 + \beta_2 \eta_{p_1}(t), \tag{11}$$

with $\mathbf{x}_{zf}(t) = [\mathbf{x}_{pf_1}(t), \mathbf{x}_{pf_3}(t)]^\top$,

$$\alpha_2 = \begin{bmatrix} \mathbf{x}_{pf_3}(t) \\ c\big(\mathbf{x}_{pf_2}(t)\big) u_{p_1}(t)/m - g \end{bmatrix},$$
$$\beta_2 = \begin{bmatrix} 0 \\ c\big(\mathbf{x}_{pf_2}(t)\big)/m \end{bmatrix}.$$

Two observers will be designed for systems (10) and (11) to estimate the unknown fault vector $\bar{\eta}_p(t)$, based on the knowledge of the measurement states $\mathbf{y}_{pf}(t)$ and the input $\mathbf{u}_p(t)$, as follows

$$\begin{aligned} \dot{\hat{\mathbf{x}}}_{\phi f}(t) &= \alpha_1 + \beta_1 \hat{\eta}_{p_2}(t) - L_{y_1} \mathbf{e}_{\phi y}(t), \\ \dot{\hat{\eta}}_{p_2}(t) &= -L_{f_1} \beta_1^\top \mathbf{e}_{\phi y}(t), \end{aligned} \tag{12}$$

with $\mathbf{e}_{\phi y}(t) = [\mathbf{y}_{pf_2}(t) - \hat{\mathbf{y}}_{pf_2}(t), \mathbf{y}_{pf_4}(t) - \hat{\mathbf{y}}_{pf_4}(t)]^\top$, and

$$\begin{aligned} \dot{\hat{\mathbf{x}}}_{zf}(t) &= \alpha_2 + \beta_2 \hat{\eta}_{p_1}(t) - L_{y_2} \mathbf{e}_{zy}(t), \\ \dot{\hat{\eta}}_{p_1}(t) &= -L_{f_2} \beta_2^\top \mathbf{e}_{zy}(t). \end{aligned} \tag{13}$$

with $\mathbf{e}_{zy}(t) = [\mathbf{y}_{pf_1}(t) - \hat{\mathbf{y}}_{pf_1}(t), \mathbf{y}_{pf_3}(t) - \hat{\mathbf{y}}_{pf_3}(t)]^\top$.

The estimation error vector is denoted by $\mathbf{e}_{py}(t) = \mathbf{y}_{pf}(t) - \hat{\mathbf{y}}_{pf}(t)$ and the observer gains are represented by $L_{y_1}, L_{y_2}, L_{f_1}$ and $L_{f_2}$. Therefore from [32] the following proposition can be stated in order to ensure the existence of the adaptive observers.

*Proposition 1: Consider the systems* (10) *and* (11) *in the adaptive observer form with no unmeasurable states. Then, for any initial conditions* $\mathbf{x}_{pf}(0)$ *and* $\hat{\mathbf{x}}_{pf}(0)$*, and any measurable bounded input* $\mathbf{u}_p(t)$*, there exists two obsevers* (12) *and* (13)*, such that the Euclidean norm of the estimation error* $\mathbf{e}_{py}(t) = \|\mathbf{y}_{pf}(t) - \hat{\mathbf{y}}_{pf}(t)\|$ *asymptotically converges to zero as t tends to infinity, while* $\mathbf{e}_{\bar{\eta}}(t) = \|\bar{\eta}_p(t) - \hat{\bar{\eta}}_p(t)\|$ *remains bounded. Also, if the time derivatives of* $\beta_1$ *and* $\beta_2$ *are bounded, then* $\mathbf{e}_{\bar{\eta}}(t) \underset{t\to\infty}{\to} 0$.

*Proof:* The proof of the Proposition 1 can be seen in [32]. □

### B. FE USING A LINEAR PIO FOR THE PVTOL AIRCRAFT

A linear proportional-integral observer will be now applied to the PVTOL aircraft in order to estimate the actuator fault vector $\bar{\eta}_p(t)$. Subsystems (3a) and (3b) are rewritten in the augmented faulty linear form using Assumption 2, with a disturbance signal $\mathbf{w}_p(t)$, as follows

$$\begin{aligned} \dot{\mathbf{x}}_{\breve{a}}(t) &= \bar{\bar{A}} \mathbf{x}_{\breve{a}}(t) + \bar{\bar{B}} \mathbf{u}_p(t) + \bar{\bar{\Gamma}} \mathbf{w}_p(t) + \bar{\mathbf{g}}, \\ \mathbf{y}_{pf}(t) &= \bar{\bar{C}} \mathbf{x}_{\breve{a}}(t), \end{aligned} \tag{14}$$

with

$$\mathbf{x}_{\breve{a}}(t) = \begin{bmatrix} \mathbf{x}_{pf}(t) \\ \bar{\eta}_p(t) \end{bmatrix}, \quad \bar{\bar{A}} = \begin{bmatrix} \breve{A} & \breve{E} \\ 0_{2\times 4} & 0_{2\times 2} \end{bmatrix}, \quad \bar{\bar{B}} = \begin{bmatrix} \breve{B} \\ 0_{2\times 2} \end{bmatrix}$$
$$\bar{\bar{\Gamma}} = \begin{bmatrix} \breve{W} \\ 0_{2\times 1} \end{bmatrix}, \quad \bar{\mathbf{g}} = \begin{bmatrix} \mathbf{g} \\ 0_{2\times 1} \end{bmatrix}, \quad \bar{\bar{C}} = \begin{bmatrix} \breve{C} \\ 0_{2\times 4} \end{bmatrix}^\top,$$

and

$$\breve{A} = \begin{bmatrix} 0_{2\times 2} & I_2 \\ 0_{2\times 2} & 0_{2\times 2} \end{bmatrix}, \quad \breve{B} = \begin{bmatrix} 0_{2\times 2} \\ J_p \end{bmatrix}, \quad \breve{C} = I_4,$$

$J_p = \mathsf{diag}(1/m, l/J_x)$, $\mathbf{g} = [0, 0, -g, 0]^\top$, where $\breve{E}$ and $\breve{W}$ introduce known matrices. Based on [33], a linear PIO can be written in the following augmented form as

$$\begin{aligned} \dot{\hat{\mathbf{x}}}_{\breve{a}}(t) &= \bar{\bar{A}} \hat{\mathbf{x}}_{\breve{a}}(t) + \bar{\bar{B}} \mathbf{u}_p(t) + \bar{\bar{L}}_{PI} \mathbf{e}_{py}(t) + \bar{\mathbf{g}}, \\ \hat{\mathbf{y}}_{pf}(t) &= \bar{\bar{C}} \hat{\mathbf{x}}_{\breve{a}}(t), \end{aligned} \tag{15}$$

where $\bar{\bar{L}}_{PI} = [\breve{L}_P, \breve{L}_I]^\top$ represents the observer gain to be computed for estimate $\bar{\eta}_p(t)$ and $\mathbf{x}_{pf}(t)$. From (14) and (15), the dynamics of the state estimation error $\mathbf{e}_{\breve{a}}(t) = \mathbf{x}_{\breve{a}}(t) - \hat{\mathbf{x}}_{\breve{a}}(t)$ is represented by

$$\dot{\mathbf{e}}_{\breve{a}}(t) = (\bar{\bar{A}} - \bar{\bar{L}}_{PI} \bar{\bar{C}}) \mathbf{e}_{\breve{a}}(t) + \bar{\bar{\Gamma}} \mathbf{w}_p(t). \tag{16}$$

The following result gives a sufficient LMI condition to guarantee the global asymptotic convergence of $\mathbf{e}_{\breve{a}}(t) \to 0$, if $\mathbf{w}_p(t) = 0$. Simultaneously, it ensures a bounded ratio of the energy of the disturbance signal, the states and the fault estimation errors, when $\mathbf{w}_p(t) \neq 0$.

*Theorem 2: The state and the fault estimation error* $\mathbf{e}_{\breve{a}}(t)$ *converge asymptotically to zero and the* $\mathcal{L}_2$*-gain of transfer from* $\mathbf{w}_q(t)$ *to* $\mathbf{e}_{\breve{a}}(t)$ *is bounded by* $\gamma > 0$ *if* $\exists\, P, M$ *and* $\gamma$*. M represents a matrix, P defines a symmetric positive definite matrix, and* $\gamma$ *is a scalar solution to the following optimization problem*

$$\min_{P,\, M} \quad \gamma, \tag{17}$$

*subject to*

$$\begin{bmatrix} \mathsf{He}\{P\bar{\bar{A}} - M\bar{\bar{C}}\} + I & P\bar{\bar{\Gamma}} \\ \bar{\bar{\Gamma}}^\top P & -\gamma^2 I \end{bmatrix} < 0, \tag{18}$$

*where* $\mathsf{He}\{P\breve{\bar{A}} - M\breve{\bar{C}}\} = (P\breve{\bar{A}} - M\breve{\bar{C}}) + (P\breve{\bar{A}} - M\breve{\bar{C}})^\top$ *and* $I$ *is an identity matrix. The gain of the observer is computed by* $\breve{\bar{L}}_{PI} = P^{-1}M$.

*Proof:* Let us choose the following candidate quadratic Lyapunov function as: $V\big(\mathbf{e}_{\breve{a}}(t)\big) = \mathbf{e}_{\breve{a}}^\top(t)P\mathbf{e}_{\breve{a}}(t)$ with $P = P^\top > 0$. Then, by defining $M = P\breve{\bar{L}}_{PI}$, the time derivative of the function $V\big(\mathbf{e}_{\breve{a}}(t)\big)$ is given by

$$\begin{aligned}\dot{V}\big(\mathbf{e}_{\breve{a}}(t)\big) = \mathbf{e}_{\breve{a}}^\top(t)(P\breve{\bar{A}} + \breve{\bar{A}}^\top P - M\breve{\bar{C}} - M^\top\breve{\bar{C}}^\top)\mathbf{e}_{\breve{a}}(t)\\ +\mathbf{e}_{\breve{a}}^\top(t)(P\breve{\Gamma})\mathbf{w}_p(t) + \mathbf{w}_p^\top(t)(\breve{\Gamma}^\top P)\mathbf{e}_{\breve{a}}(t). \quad (19)\end{aligned}$$

The objective is to minimize the $\mathcal{L}_2$-gain of the transfer from $\mathbf{w}_p(t)$ on the error $\mathbf{e}_{\breve{a}}(t)$. This is formulated by $\|\mathbf{e}_{\breve{a}}(t)\|_2 < \gamma\|\mathbf{w}_p(t)\|_2$. The above implies to compute the observer gain matrix $\breve{\bar{L}}_{PI}$ to stabilize the error system (16) and ensures asymptotic convergence of the state and the fault estimation error to zero when the perturbation is null, $\mathbf{w}_p(t) = 0$. Likewise to attenuate the transfer gain from the bounded perturbation to the state and fault estimation error when the perturbation is different from zero $\mathbf{w}_p(t) \neq 0$. This problem can be formulated as follows:

$$\dot{V}\big(\mathbf{e}_{\breve{a}}(t)\big) + \mathbf{e}_{\breve{a}}(t)^\top\mathbf{e}_{\breve{a}}(t) - \gamma^2\mathbf{w}_p(t)^\top\mathbf{w}_p(t) < 0. \quad (20)$$

By substituting $\dot{V}\big(\mathbf{e}_{\breve{a}}(t)\big)$ from (19), the stability conditions (20) can be rewritten as

$$\Upsilon^\top\begin{bmatrix}\mathsf{He}\{P\breve{\bar{A}} - M\breve{\bar{C}}\} + I & P\breve{\bar{\Gamma}}\\ \breve{\bar{\Gamma}}^\top P & -\gamma^2 I\end{bmatrix}\Upsilon < 0. \quad (21)$$

with $\Upsilon = [\mathbf{e}_{\breve{a}}(t), \mathbf{w}_p(t)]^\top$.

Then, the inequality (21) is negative definite if condition (18) is fulfilled. Finally, the LMI in Theorem 2 is obtained. This completes the proof. □

### C. FE USING A qLPV PIO FOR THE QUADCOPTER VEHICLE

Let consider the rotational part of the quadcopter model (1a) and the sector-nonlinearity technique [34]. Then (1a) can be rewritten as the nonlinear state-space form as follows

$$\begin{aligned}\dot{\mathbf{x}}_r(t) &= A\big(\dot{\phi}_q(t), \dot{\theta}_q(t)\big)\mathbf{x}_r(t) + B\mathbf{u}_r(t),\\ &\quad +W\big(\dot{\phi}_q(t), \dot{\theta}_q(t)\big)\mathbf{w}_r(t),\\ \mathbf{y}_r(t) &= C\mathbf{x}_r(t), \end{aligned} \quad (22)$$

with

$$\begin{aligned}A\big(\dot{\phi}_q(t), \dot{\theta}_q(t)\big) &= \begin{bmatrix}0_{3\times3} & I_3\\ 0_{3\times3} & A_r\end{bmatrix}, \quad C = I_6,\\ W\big(\dot{\phi}_q(t), \dot{\theta}_q(t)\big) &= \big[0_{3\times1}, b_1\dot{\theta}_q(t), b_2\dot{\phi}_q(t), 0\big]^\top,\\ A_r &= \begin{bmatrix}0 & 0 & h_1\dot{\theta}_q(t)\\ 0 & 0 & h_2\dot{\phi}_q(t)\\ h_3\dot{\theta}_q(t) & 0 & 0\end{bmatrix}, \quad B = \begin{bmatrix}0_{3\times3}\\ J_r\end{bmatrix},\end{aligned}$$

$J_r = \mathsf{diag}(l/J_x, l/J_y, d/J_z)$, $h_1 = (J_y - J_z)/J_x$, $h_2 = (J_z - J_x)/J_y$, $h_3 = (J_x - J_y)/J_z$, $b_1 = -J_{rz}/J_x$ and $b_2 = J_{rz}/J_y$. The state vector is defined as $\mathbf{x}_r(t) = [\phi_q(t), \theta_q(t), \psi_q(t), \dot{\phi}_q(t), \dot{\theta}_q(t), \dot{\psi}_q(t)]^\top$ and $\mathbf{w}_r(t) = \Omega_M(t)$ is the disturbance vector. The number of local linear models is directly related to the number of the nonlinear terms. For each nonlinear term, two sub-models are obtained such that for $\bar{p}$ nonlinear terms, the global model is composed of $k = 2^{\bar{p}}$ sub-models.

*Remark 2:* From a practical point of view, it is difficult to measure overall residual propeller angular speed $\Omega_M(t)$. Thus, in this paper, it is considered as a perturbation $\mathbf{w}_r(t)$ acting on the quadcopter system.

The scheduling variables $\zeta(t) = [\zeta_1(t), \zeta_2(t)]^\top$, which are the non-constant elements in (22), are: $\zeta_1(t) = \dot{\phi}_q(t) \in [-\pi/2,\ \pi/2]$ (rad/s), and $\zeta_2(t) = \dot{\theta}_q(t) \in [-\pi/2,\ \pi/2]$ (rad/s). For each scheduling variable, two weighting functions are computed as follows

$$\begin{aligned}\mu_0^1 &= \big(\pi - 2\dot{\phi}_q(t)\big)/2\pi, \quad \mu_1^1 = 1 - \mu_0^1,\\ \mu_0^2 &= \big(\pi - 2\dot{\theta}_q(t)\big)/2\pi, \quad \mu_1^2 = 1 - \mu_0^2.\end{aligned} \quad (23)$$

Therefore, for $\bar{p} = 2$, $k = 4$ scheduling functions are computed as the product of the weighting functions that correspond to each local model, as follows

$$\begin{aligned}\rho_1(\zeta(t)) = \mu_0^1\mu_0^2, \quad \rho_2(\zeta(t)\big) = \mu_0^1\mu_1^2,\\ \rho_3(\zeta(t)\big) = \mu_1^1\mu_0^2, \quad \rho_4(\zeta(t)\big) = \mu_1^1\mu_1^2,\end{aligned} \quad (24)$$

satisfying the following convex set sum property

$$\rho_i\big(\zeta(t)\big) \geq 0, \quad \sum_{i=1}^{4}\rho_i\big(\zeta(t)\big) = 1,\ \forall t, \forall i = 1, \ldots, 4. \quad (25)$$

The known matrices $A_i$ and $W_i$, with $i = 1, \ldots, 4$ (defining the 4 sub-models) are computed by replacing the scheduling variables $\zeta(t)$ to the matrices $A(\dot{\phi}_q(t), \dot{\theta}_q(t))$ and $W(\dot{\phi}_q(t), \dot{\theta}_q(t))$ with the scalars $\zeta_j^{\Lambda_i^j}$, with $i = 1, \ldots, 4$ and $j = 1, 2$:

$$A_i = A\big(\zeta_1^{\Lambda_i^1}, \zeta_2^{\Lambda_i^2}\big), \qquad W_i = W\big(\zeta_1^{\Lambda_i^1}, \zeta_2^{\Lambda_i^2}\big), \quad (26)$$

where the indexes $\Lambda_i^j$ ($i = 1, \ldots, 4$ and $j = 1, 2$) denote the minimum and maximum scalar values of $\zeta_j(t)$ and indicate which portion of the $j$–th scheduling variable ($\mu_0^j$ or $\mu_1^j$) is involved in the $i$–th sub-model. Consequently, by using the scheduling functions given by (24), the rotational part of the nonlinear system (1) is exactly represented only in the selected segment, by the following qLPV model

$$\begin{aligned}\dot{\mathbf{x}}_r(t) &= \textstyle\sum_{i=1}^4 \rho_i\big(\zeta(t)\big)\big(A_i\mathbf{x}_r(t) + B\mathbf{u}_r(t) + W_i\mathbf{w}_r(t)\big),\\ \mathbf{y}_r(t) &= C\mathbf{x}_r(t).\end{aligned} \quad (27)$$

Following the same procedure as in the previous subsection, system (27) is rewritten in an augmented faulty qLPV form as

$$\begin{aligned}\dot{\mathbf{x}}_a(t) &= \sum_{i=1}^{4}\rho_i\big(\zeta(t)\big)\big(\bar{A}_i\mathbf{x}_a(t) + \bar{B}\mathbf{u}_r(t) + \bar{\Gamma}_i\mathbf{w}_r(t)\big),\\ \mathbf{y}_{rf}(t) &= \bar{C}\mathbf{x}_a(t),\end{aligned} \quad (28)$$

with

$$\mathbf{x}_a(t) = \begin{bmatrix}\mathbf{x}_{rf}(t)\\ \bar{\eta}_r(t)\end{bmatrix}, \quad \bar{A}_i = \begin{bmatrix}A_i & E\\ 0_{3\times6} & 0_{3\times3}\end{bmatrix}, \quad \bar{B} = \begin{bmatrix}B\\ 0_{3\times3}\end{bmatrix}$$

$$\bar{\Gamma}_i = \begin{bmatrix}W_i\\ 0_{3\times1}\end{bmatrix}, \quad \bar{C} = \begin{bmatrix}C\\ 0_{3\times6}\end{bmatrix}^\top, \quad \bar{\eta}_r(t) = \begin{bmatrix}\eta_{q2}(t)\\ \eta_{q3}(t)\\ \eta_{q4}(t)\end{bmatrix}.$$

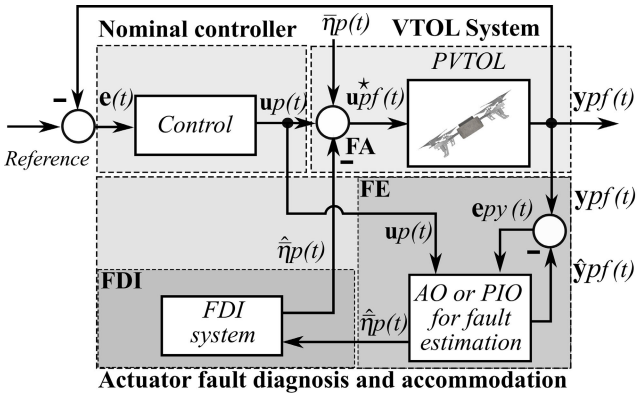


**FIGURE 2.** FA scheme applied to the PVTOL aircraft.

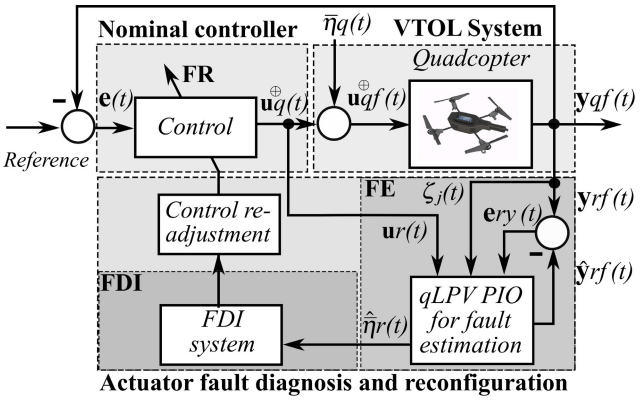


**FIGURE 3.** FR scheme applied to the quadcopter vehicle.

An extension of classical PI observer for the qLPV system (28) is written in the augmented form as

$$\begin{aligned}\dot{\hat{\mathbf{x}}}_a(t) &= \sum_{i=1}^{4} \rho_i\big(\zeta(t)\big)\big(\bar{A}_i\hat{\mathbf{x}}_a(t) + \bar{B}\mathbf{u}_r(t) + \bar{L}_{PIi}\mathbf{e}_{ry}(t)\big),\\ \hat{\mathbf{y}}_{rf}(t) &= \bar{C}\hat{\mathbf{x}}_a(t),\end{aligned} \tag{29}$$

where $\mathbf{e}_{ry}(t) = \mathbf{y}_{rf}(t) - \hat{\mathbf{y}}_{rf}(t)$ is the estimation error vector, $\bar{L}_{PIi} = [L_{Pi}, L_{Ii}]^\top$ represents the observer gain. The dynamics of the state estimation error $\mathbf{e}_a(t) = \mathbf{x}_a(t) - \hat{\mathbf{x}}_a(t)$ between (28) and (29) is given by

$$\dot{\mathbf{e}}_a(t) = \sum_{i=1}^{4} \rho_i\big(\zeta(t)\big)\big((\bar{A}_i - \bar{L}_{PIi}\bar{C})\mathbf{e}_a(t) + \bar{\Gamma}_i\mathbf{w}_r(t)\big). \tag{30}$$

The problem of the robust state and fault estimation error is reduced to determine the matrices $\bar{L}_{PIi}$ with the same characteristics applied in the design of the liner PIO, summarized in Theorem 2. Now, Theorem 2 can be applied to the rotational dynamics of the quadcopter vehicle using (30), considering the scheduling functions (24) and the known matrices $A_i$ and $W_i$ (26).

## V. FAULT TOLERANT CONTROL SCHEMES

The fast dynamics of the VTOL systems represent a challenge for fault detection quickly before the vehicle crashes. Our interest is to validate experimentally the fesibility in real time of the proposed fault estimators into an active FTC algorithm for VTOL systems. In order to achieve this goal a Fault Accommodation (FA) and Fault Reconfiguration (FR) schemes are proposed. In Figs. 2 and 3 general FA and FR structures for the PVTOL and quadcopter system are depicted, respectively. FA strategy is applied to the PVTOL and the quadcopter system in the presence of a soft fault while FR is only applied to the quadcopter suffering an aggressive fault. Notice here that the schemes are composed of three main blocks; i) the VTOL system, ii) the nominal controller and iii) the actuator fault diagnosis (FE and Fault Detection and Isolation (FDI) system) and the accommodation or reconfiguration system.

When the vehicle is flying in the fault-free case only the nominal controller is applied. Once the fault occurs, the FE signals generated by the observer (AO, PIO or qLPV PIO) are used to detect, isolate and accommodate or reconfigure the actuator fault. The actuator fault is detected when any additive FE signal has a greater value than a predefined threshold. When this occurs, the sign value of the FE is considered to isolate the fault. Finally, FTC law is computed using the FE vector, when the fault is detected (faulty case) and isolated.

### A. NOMINAL CONTROLLER

For simplify the validation procedure, we have chosen the following PD controller based on unit quaternions

$$\mathbf{u}_\vartheta(t) = \begin{bmatrix} \| - K_{P\xi}\big(\xi(t) - \xi_d(t)\big) - K_{D\xi}\big(\bar{v}(t) - \bar{v}_d(t)\big)\| \\ -2K_{P\Omega}\ln\big(\mathrm{q}_e(t)\big) - K_{D\Omega}\big(\Omega(t) - \Omega_d(t)\big) \end{bmatrix} \tag{31}$$

The tuning parameters of the controller (31) are represented by $K_{P\xi} = \mathrm{diag}(k_{P\bar{\xi}})$, $K_{D\xi} = \mathrm{diag}(k_{D\bar{\xi}})$, $K_{P\Omega} = \mathrm{diag}(k_{P\bar{\Omega}})$, and $K_{D\Omega} = \mathrm{diag}(k_{D\bar{\Omega}})$, with $\bar{\xi} = \{x, y, z\}$, and $\bar{\Omega} = \{\phi, \theta, \psi\}$. The quaternion error between the actual orientation and the desired reference is $\mathrm{q}_e(t)$, and $\bar{v}(t)$ describes the linear velocity of the vehicle. The subscript $d$ indicates the reference. The nominal control law for the PVTOL system is the same as (31) assuming that the quadcopter degree-of-freedoms for pitch and yaw have been previously stabilized. This means that PVTOL aircraft configuration is achieved when choosing the quadcopter references for $\psi_q(t)$ and $x_q(t)$ equal to 0, i.e., $\psi_q(t), \theta_q(t), x_q(t) = 0, \forall t$.

*Remark 3:* The quaternion-based PD controller (31) is only used to show the effectiveness of the proposed FE system. The study of the controller is out of the scope of this work, more details could be found in [35].

### B. FDI SYSTEM

The additive fault estimation components of the vector are used to detect any actuator faults, as follows:

$$\begin{aligned} |\bar{\eta}_{\vartheta_{\bar{j}}}(t)| &\geq T_{\vartheta_{\bar{j}}} \quad \Rightarrow \text{in faulty case (Alarm = 1)},\\ |\bar{\eta}_{\vartheta_{\bar{j}}}(t)| &< T_{\vartheta_{\bar{j}}} \quad \Rightarrow \text{in fault-free case (Alarm = 0)}, \end{aligned} \tag{32}$$

where $T_{\vartheta_{\bar{j}}}$ are constant thresholds defined for the PVTOL ($\bar{j} = 1, 2$), and the quadcopter ($\bar{j} = 2, 3, 4$), chosen according to experimental results. In fault-free case the estimated value $|\bar{\eta}_{\vartheta_{\bar{j}}(t)}|$ is close to zero, while in faulty case the estimated value

**TABLE 3.** Fault isolation logic.

| PVTOL[1] | | |
|---|---|---|
| Faults | $\hat{\eta}_{p_1}(t)$ | $\hat{\eta}_{p_2}(t)$ |
| $\{M_1, M_4\}$ | - | - |
| $\{M_2, M_3\}$ | - | + |
| $\{M_1, M_2, M_3, M_4\}$ | + | 0 |

| Quadcopter | | | |
|---|---|---|---|
| Faults | $\hat{\eta}_{q_2}(t)$ | $\hat{\eta}_{q_3}(t)$ | $\hat{\eta}_{q_4}(t)$ |
| $M_1$ | - | - | + |
| $M_2$ | + | - | - |
| $M_3$ | + | + | + |
| $M_4$ | - | + | - |

[1] PVTOL: Planar Vertical Take-Off and Landing.

has a greater value than a threshold, for indicating a fault occurrence. If any component of the vector is greater than the threshold then it is considered a faulty case and the alarm indicator is one. From (6) and (7), it is clear that the additive faults can be either positive or negative depending on the faulty actuator. Nevertheless, the fault produced on the main thrust is always negative. Therefore, from the previous, it is possible to generate Table 3 for isolating the actuator faults in both systems. From this table, zero indicates no change in the signal, sign + or − indicates a positive or negative value of the estimated signal.

### C. FA CONTROL LAW

Once the partial fault is detected, a new control law is added to the nominal control law to compensate the fault effect on the system. The goal here is to use the FE signal to generate this new control law and ensure the tracking trajectory performance of the faulty system to the reference one. By using (6) the FA control law is given by the following equations:

$$\mathbf{u}^{\star}_{\vartheta f}(t) = \mathbf{u}_{\vartheta f} - \hat{\bar{\eta}}_{\vartheta}(t), \tag{33}$$

where the first part of equation (33) is the input vector with actuator faults and the second part is the compensation control to be added in order to accommodate the actuator fault, see Fig. 2. For example, for the case of the quadcopter vehicle, note that the qLPV PIO (29) only provides $\hat{\bar{\eta}}_r(t)$ because it is applied to the attitude dynamics. Then, to compute the FA control law (33) the value of FE in roll dynamics is applied as follows

$$\hat{\bar{\eta}}_q(t) = [-|\hat{\eta}_{q_2}(t)|, \hat{\bar{\eta}}_r(t)]^{\top}. \tag{34}$$

Nevertheless, any fault estimation signal $\hat{\eta}_{q_3}(t)$ or $\hat{\eta}_{q_4}(t)$ can be used. To make the reader better understand this strategy, suppose a partial fault in the motor $M_2$ of the quadcopter. Next, according to (7), $\lambda_1(t)$, $\lambda_3(t)$ and $\lambda_4(t)$ are equal to zero and the actuator fault vector is represented by

$$\begin{aligned}\bar{\eta}_q(t) &= [\eta_{q_1}(t), \eta_{q_2}(t), \eta_{q_3}(t), \eta_{q_4}(t)]^{\top} \\ &= [-\lambda_{q_2}(t)f_{q_2}(t), \lambda_{q_2}(t)f_{q_2}(t), \\ &\quad -\lambda_{q_2}(t)f_{q_2}(t), -\lambda_{q_2}(t)f_{q_2}(t)]^{\top}.\end{aligned} \tag{35}$$

Then, from (35) it is clear that fault isolation can be done by analyzing the sign value of the components of $\hat{\bar{\eta}}_r$, as it is shown in Table 3. Finally, FA control law (33) using (34) can be applied.

**TABLE 4.** Controller and AO parameters.

| | |
|---|---|
| $L_{y_1} = 0.009$ | $L_{f_1} = 50$ |
| $L_{y_2} = 5$ | $L_{f_2} = 50$ |
| $K_{P\xi} = \text{diag}(0.18, 0.18, 0.52)$ | $K_{D\xi} = \text{diag}(0.08, 0.08, 0.22)$ |
| $K_{P\Omega} = \text{diag}(1.5, 1.5, 2)$ | $K_{D\Omega} = \text{diag}(0.2, 0.2, 0.5)$ |

### D. FR CONTROL LAW FOR AGGRESSIVE FAULTS

The proposed fault reconfiguration strategy deals with an aggressive fault presented only in the quadcopter vehicle, where the structure of the loop is changed in order to ensure fault tolerance. By using the controllability analysis presented in Table 2, the following strategy is stated. When the fault is correctly detected and isolated, the control re-adjustment module uses this information to modify the parameters of the orientation controller, controlling yaw velocity but leaving the yaw angle without control, see Fig. 3. This implies that the quadcopter will be spinning around $z_q$-axis with a constant velocity. The physical position of the faulty actuator determines the direction of the spinning rotation $\bar{h}$ while the speed of rotation $\dot{\bar{\psi}}$ depends on the yaw damping coefficient of the quadcopter. The FR strategy includes the following two steps:

Step 1: Once the fault is detected, the parameters of the orientation controller are changed and $k_{P\psi}$ is set to zero, leaving yaw angle uncontrolled.

Step 2: When the fault is correctly isolated the reference of yaw velocity is changed to $\dot{\psi}_d(t) = \bar{h}\dot{\bar{\psi}}$, where $\bar{h} = 1$ for faults presented in $M_1$ or $M_3$ and $\bar{h} = -1$ for faults in $M_2$ or $M_4$.

## VI. EXPERIMENTAL RESULTS

The Parrot AR Drone 2.0 was chosen as the prototype for performing tests in real time. This commercial vehicle has been adapted to work under our framework which runs into a Linux-based operation system, capable of implementing a wide range of control algorithms.

Observer gains for (15) and (29) are obtained by solving the LMI of the Theorem 2 using the Yalmip Toolbox [36]. The attenuation level for each observer is $\gamma = 0.064$. This value guarantees an adequate performance of the observer and its robustness against disturbances. The parameters of the nonlinear AO and the nominal controller are introduced in Table 4. For testing the effectiveness of the proposed scheme, four scenarios were considered. We refer the reader to Appendix, for videos of experimental results.

### A. SCENARIO 1 - PVTOL: HOVER FLIGHT

In the first scenario the vehicle is flying at hover position and a constant partial fault of 30% is injected in the motors $M_1$ and $M_4$ ($f_{p_1}$) applied at time 2.8 s. At 22.8 s the fault is removed. Then, from 32.8 s to 52.7 s a fault of 30% is imposed in all motors.

In Fig. 4 a comparison between the faulty PVTOL aircraft with and without the proposed FA scheme using the FE generated by the PIO and AO is displayed. Notice from this

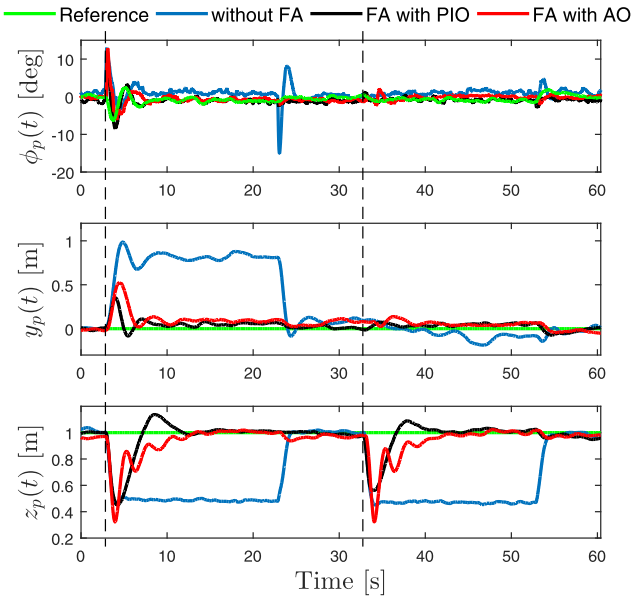


**FIGURE 4.** Scenario 1 - Position and Euler angle comparison between the faulty PVTOL with and without FA.

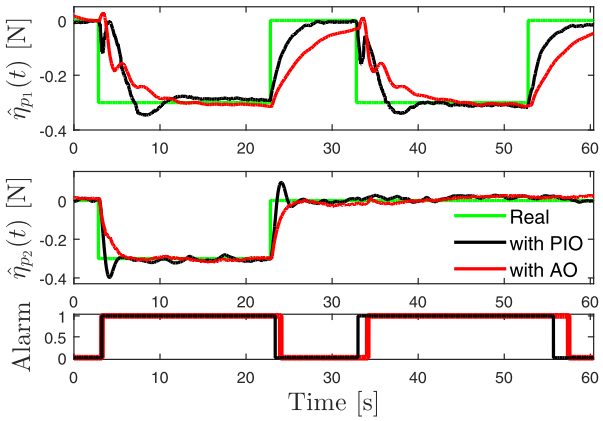


**FIGURE 5.** Scenario 1 - Additive fault estimation and alarm indicator.

figure that when the FA strategy is applied the PVTOL attitude, position and altitude tracking performance is recovered shortly after the occurrence of the two and four simultaneous actuator faults. In Fig. 5 the estimated additive fault and the fault detection used for generating the FA control law (33) are introduced. Observe here that shortly after the fault is injected, the magnitude estimation reasonably approximates the true fault magnitude. In Fig. 6 the forces produced by the actuators with the proposed FA scheme using the AO and the PIO are presented. Observe that all forces are under actuator saturation. Nevertheless, FA performance using the PIO can generate the required forces faster than the AO algorithm, so as to properly mitigate the actuator faults with less time delay.

In order to compare the observer performances, the Integral of Absolute Error (IAE) is obtained for the tracking and fault estimation error.

Table 5 shows that the minimum values of the IAE are obtained for the linear PIO. These results show that the PIO

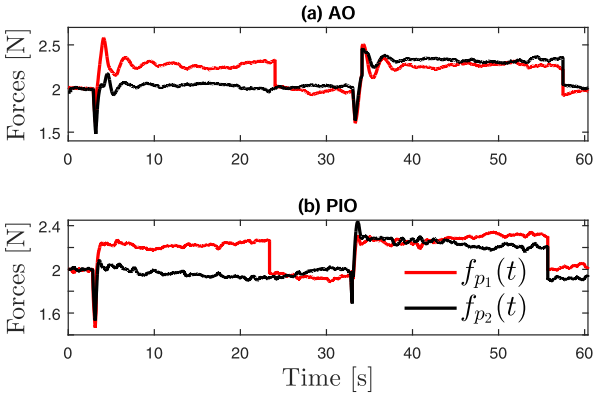


**FIGURE 6.** Scenario 1 - Forces generated by the actuators with the proposed FA scheme using (a) AO and (b) PIO.

**TABLE 5.** Performance indexes of the linear PIO and AO applied to the PVTOL aircraft.

| Quality indicator IAE[1] | | |
|---|---|---|
| Error | Observer | |
| | PIO[1] | AO[1] |
| $\phi_p(t) - \phi_{p_d}(t)$ | 0.74 | 1.03 |
| $y_p(t) - y_{p_d}(t)$ | 2.72 | 4.59 |
| $z_p(t) - z_{p_d}(t)$ | 3.48 | 4.12 |
| $\eta_{p_1}(t) - \hat{\eta}_{p_1}(t)$ | 2.77 | 4.22 |
| $\eta_{p_2}(t) - \hat{\eta}_{p_2}(t)$ | 1.07 | 1.26 |

[1] IAE: Integral of Absolute Error, PIO: Proportional-Integral Observer, AO: Adaptive Observer.

presents better performance for fault estimation compared to the AO. Thus, an extension of the linear PIO to the qLPV PIO for fault estimation is applied to the quadcopter vehicle, by considering the nonlinearities of the system.

### B. SCENARIO 2 - QUADCOPTER: HOVER FLIGHT

This scenario was developed as follows: when the vehicle is flying at hover position $(x_d, y_d, z_d) = (0, 0, 1)$ m, a partial fault of 13%, applied approximately at time 8.51 s, is artificially injected in motor $M_1$.

In Fig. 7 position and Euler angles comparison between the faulty quadcopter vehicle with and without the FA strategy is presented. Notice from this figure that when a partial fault is applied the quadcopter loses performance and the nominal control law is not capable to recover the desired position. Nevertheless, when the FA scheme is applied, system performance is improved and the FTC recovers satisfactorily the desired position. In addition, when the FA system is not used, the quadcopter becomes unstable and it was necessary, for vehicle safety, to carry out an emergency landing, as can be seen in Fig. 7. Fig. 8 illustrates the fault estimation. Observe that the fault estimation reasonably approximates the true fault magnitude. Before the occurrence of an actuator fault, all the additive FE signals remain below their corresponding threshold, when the fault occurs, at least one fault estimation value exceeds its threshold, indicating the occurrence of an actuator fault. The actuator fault is correctly detected after 0.08 s of its occurrence.

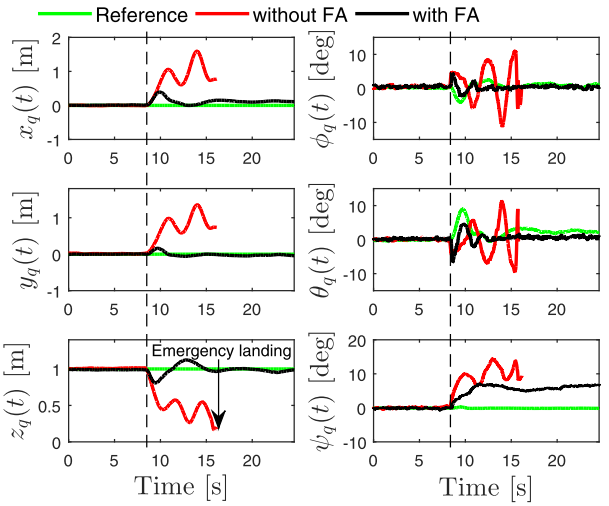


**FIGURE 7.** Scenario 2 - Position and Euler angles comparison between the faulty quadcopter without and with FA.

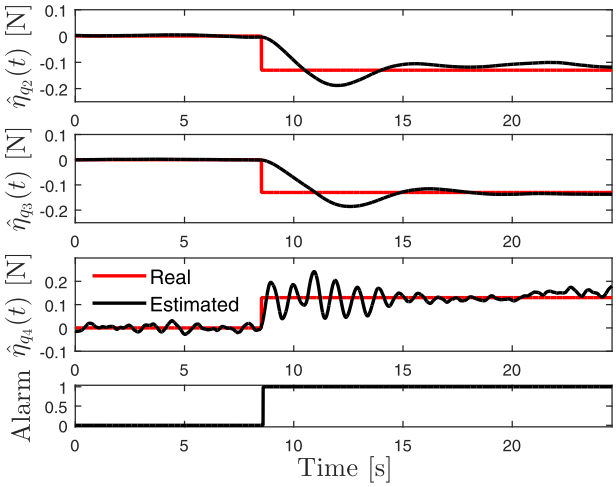


**FIGURE 8.** Scenario 2 - Additive fault estimation and alarm indicator.

Once the fault is detected, fault isolation is performed using Table 3, considering the sign of the additive fault estimation values, as shown in Fig. 8. Fault estimation $\hat{\eta}_{q_2}(t)$ and $\hat{\eta}_{q_3}(t)$ are negative while $\hat{\eta}_{q_4}(t)$ is positive due to the actuator fault. Fig. 9 shows the forces generated by the actuators when the proposed FA scheme is applied. Note from this figure, at time 8.6 s, that the commanded rotor forces corresponding to rotor $M_1$ increase to compensate the fault while the forces corresponding to rotors $M_2$, $M_3$ and $M_4$ are virtually unaffected by the occurrence of the fault.

### C. SCENARIO 3 - QUADCOPTER: CIRCULAR TRAJECTORY

The mission for the third scenario was to track a circular trajectory in a constant altitude and apply a partial fault of 12% in motor $M_2$ at time 18.49 s. The circular trajectory has a radius of 1 m and the desired altitude was 1 m.

Fig. 10 depicts the scheduling functions which represent the soft interpolation between the four models of the attitude system in order to reproduce the nonlinear behavior of the quadcopter vehicle.

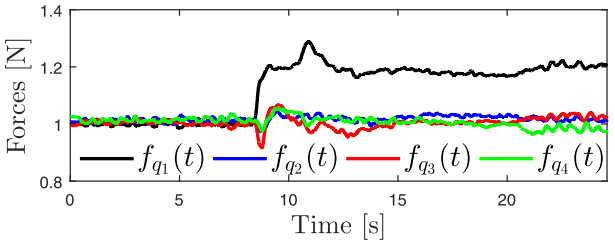


**FIGURE 9.** Scenario 2 - Forces generated by the actuators with the proposed FA scheme.

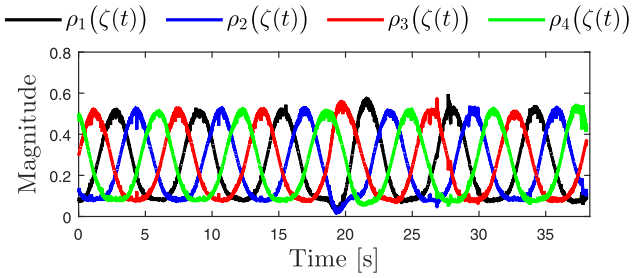


**FIGURE 10.** Scenario 3 - Gain scheduling functions.

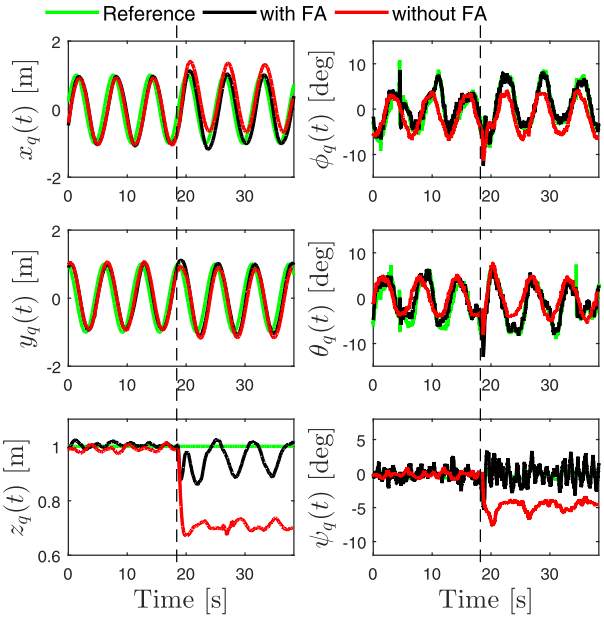


**FIGURE 11.** Scenario 3 - Position and Euler angles comparison between the faulty quadcopter without and with FA.

In Fig. 11 a states comparison between the faulty vehicle without and with the FA using the FE generated by the qLPV PIO is displayed. Clearly, the proposed strategy significantly reduces the error between the desired and the real position. The fault identification is performed correctly, as can be appreciated in Fig. 12. Observe here that the fault estimation is close to zero in the fault-free case even with the circular trajectory reference, and is close to the fault magnitude when the fault appears. The actuator fault detection is achieved after 0.18 s of its occurrence, and consequently the new control law is generated for compensate the actuator fault. The fault estimation vector is used, as discussed before, in order to

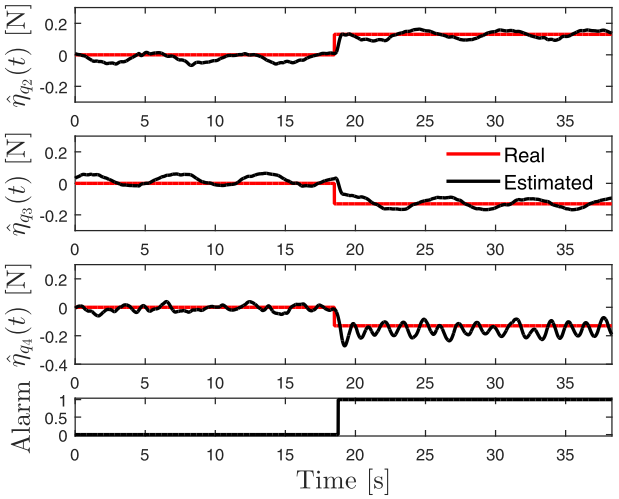


**FIGURE 12.** Scenario 3 - Additive fault estimation and alarm indicator.

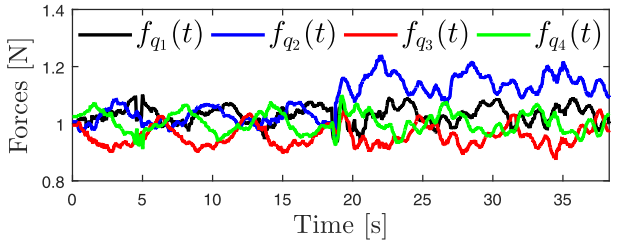


**FIGURE 13.** Scenario 3 - Forces generated by the actuators with the proposed FA scheme.

isolate the partial fault. The soft partial fault in motor $M_2$ is correctly detected, isolated and compensated applying the isolation logic presented in Table 3 and the FTC law (33). Fig. 13 shows the forces generated by the actuators. As can be seen, after the faults occur at time 18.77 s the force corresponding to rotor $M_2$ immediately responds to the presence of the fault, while the controller command corresponding to rotors $M_1$, $M_3$ and $M_4$ remains unaffected.

### D. SCENARIO 4 - QUADCOPTER: AGGRESSIVE FAULT

In order to show the feasiblity of the FE algorithm in the quadcopter suffering an aggressive fault, the proposed FR scheme is carried out. In this scenario, a loss of 80% of control effectiveness imposed in the motor $M_1$ is injected at time 7.8 s while the quadcopter is flying at hover position. When the fault is detected the gains of the orientation controller change to $K_{P\bar{\Omega}} = \text{diag}(0.8, 0.8, 0)$ and $K_{D\bar{\Omega}} = \text{diag}(0.1, 0.1, 0.2)$. Observe that the proportional gain of yaw angle is set to zero, leaving it uncontrolled. When the fault is isolated, yaw speed of rotation is set to $\dot{\bar{\psi}}(t) = 9$ (rad/s) or 515.6 (deg/s) with the direction of spinning $\bar{h}$ defined according to the actuator fault localization result.

From Fig. 14, the position comparison of the quadcopter vehicle in 3-D space is presented. This figure shows that with no FR strategy the quadcopter crashes to the ground. In contrast, the FR system allows the vehicle to finish its path successfully.

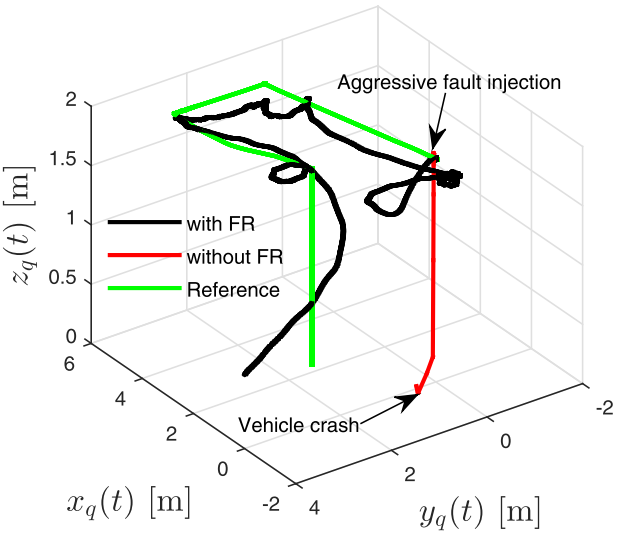


**FIGURE 14.** Scenario 4 - Position comparison between the faulty quadcopter without and with FR in 3-D space.

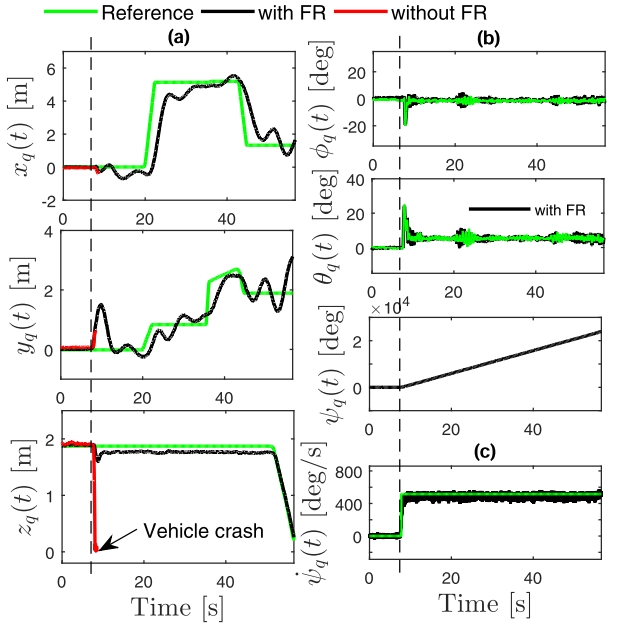


**FIGURE 15.** Scenario 4 - (a) Position, (b) Euler angles and (c) yaw velocity of the faulty quadcopter with FR.

In addition, in Fig. 15 the position and attitude dynamics are displayed. Fig. 15(b) introduces the roll $\phi_q(t)$ and pitch $\theta_q(t)$ angles that are around zero denoting a stable flight, even in presence of an aggressive fault. Also, Fig. 15(b) shows that the yaw angle changes due to the uncontrolled state. The yaw angular velocity of the vehicle during the flight test is displayed in Figure 15(c). Fault detection and isolation result is introduced in Fig. 16.

Using Table 3 is clear that the fault occurs in $M_1$. When the fault is isolated in $M_1$, the spinning direction is set to $\bar{h} = 1$ and the reference of yaw velocity $\dot{\bar{\psi}}_d = 9$ (rad/s), as shown Fig. 15(c). Fig. 17 displays the forces generated by the motors of the quadcopter when the FR algorithm is applied. It can be seen clearly that, when the fault is injected in $M_1$, the forces

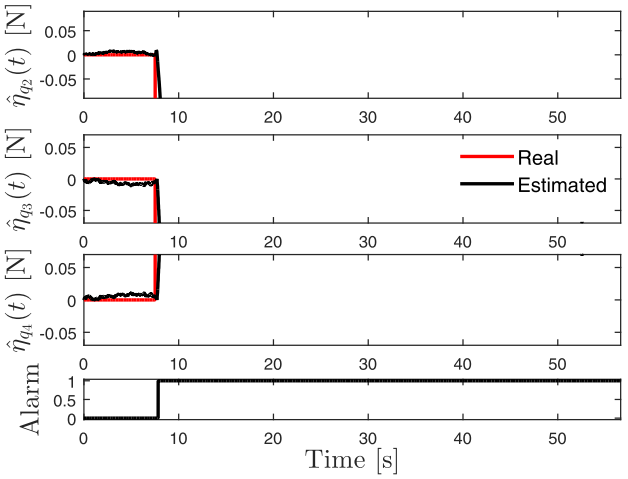


**FIGURE 16.** Scenario 4 -Fault detection and isolation performance and alarm indicator.

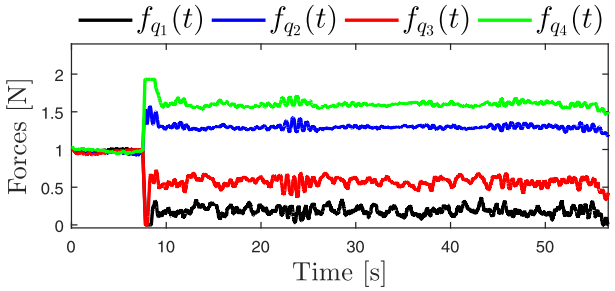


**FIGURE 17.** Scenario 4 - Forces generated by the actuators with the proposed FR scheme.

produced by the opposite motor $M_3$ reduce its magnitude and the remaining motors increase their forces rapidly in order to achieve the yaw reference velocity. Note that when the fault is reconfigured the quadcopter follows the desired path correctly and land without damage.

## VII. CONCLUSION

Actuator fault estimation strategies were proposed and validated experimentally using model-based observers for VTOL aerial vehicles. A nonlinear AO and a linear PIO have been applied to the PVTOL aircraft and a qLPV PIO was used into the quadcopter vehicle. The ACAI method was considered to analyze the controllability of the vehicles under LoE. The fault detection was done by comparing the fault estimation signal with a predefined threshold. Fault isolation was achieved by analyzing the sign of the fault estimation signal. Experimental validation of the complete active FTC schemes was carried out using the proposed FE systems in order to accommodate soft actuator faults and reconfigure aggressive faults for retaining close to nominal fault-free performance, even when the vehicle is flying in a non-hover position. Finally, experimental results have corroborated the effectiveness of the proposed FTC schemes. The results of the proposed FE strategies demonstrate that they can be applied into different active FTC schemes for VTOL aerial vehicles, even in the case of an actuator failure and flying in a non-hover position.

## APPENDIX
## VIDEOS OF EXPERIMENTAL RESULTS

Videos of experimental results can be viewed online: https://youtu.be/MsZ4w35nKS8 and https://youtu.be/7dDj7tYCjXc.

## REFERENCES

[1] J. Straub, "Unmanned aerial systems: Consideration of the use of force for law enforcement applications," *Technol. Soc.*, vol. 39, pp. 100–109, Nov. 2014.
[2] Y. Zhang, A. Chamseddine, C. Rabbath, B. Gordon, C.-Y. Su, S. Rakheja, C. Fulford, J. Apkarian, and P. Gosselin, "Development of advanced FDD and FTC techniques with application to an unmanned quadrotor helicopter testbed," *J. Franklin Inst.*, vol. 350, no. 9, pp. 2396–2422, Nov. 2013.
[3] Y. Zhang and J. Jiang, "Bibliographical review on reconfigurable fault-tolerant control systems," *Annu. Rev. Control*, vol. 32, no. 2, pp. 229–252, Dec. 2008.
[4] J. C. L. Chan, C. P. Tan, H. Trinh, M. A. S. Kamal, and Y. S. Chiew, "Robust fault reconstruction for a class of non-infinitely observable descriptor systems using two sliding mode observers in cascade," *Appl. Math. Comput.*, vol. 350, pp. 78–92, Jun. 2019.
[5] J. C. L. Chan, C. P. Tan, H. Trinh, and M. A. S. Kamal, "State and fault estimation for a class of non-infinitely observable descriptor systems using two sliding mode observers in cascade," *J. Franklin Inst.*, vol. 356, no. 5, pp. 3010–3029, Mar. 2019.
[6] M. H. Amoozgar, A. Chamseddine, and Y. Zhang, "Experimental test of a two-stage Kalman filter for actuator fault detection and diagnosis of an unmanned quadrotor helicopter," *J. Intell. Robot. Syst.*, vol. 70, nos. 1–4, pp. 107–117, Apr. 2013.
[7] H. Aguilar-Sierra, G. Flores, S. Salazar, and R. Lozano, "Fault estimation for a quad-rotor MAV using a polynomial observer," *J. Intell. Robot. Syst.*, vol. 73, nos. 1–4, pp. 455–468, Jan. 2014.
[8] Z. Cen, H. Noura, T. B. Susilo, and Y. A. Younes, "Robust fault diagnosis for quadrotor UAVs using adaptive Thau observer," *J. Intell. Robot. Syst.*, vol. 73, nos. 1–4, pp. 573–588, Jan. 2014.
[9] A.-R. Merheb and H. Noura, "Active fault-tolerant control of quadrotor uavs based on passive controller bank," in *Mechanism, Machine, Robotics and Mechatronics Sciences*. Cham, Switzerland: Springer, 2019, pp. 231–241.
[10] Y. Song, L. He, D. Zhang, J. Qian, and J. Fu, "Neuroadaptive fault-tolerant control of quadrotor UAVs: A more affordable solution," *IEEE Trans. Neural Netw. Learn. Syst.*, vol. 30, no. 7, pp. 1975–1983, Jul. 2019.
[11] X. Nian, W. Chen, X. Chu, and Z. Xu, "Robust adaptive fault estimation and fault tolerant control for quadrotor attitude systems," *Int. J. Control*, pp. 1–13, Feb. 2018.
[12] Y. Zhong, Y. Zhang, W. Zhang, J. Zuo, and H. Zhan, "Robust actuator fault detection and diagnosis for a quadrotor UAV with external disturbances," *IEEE Access*, vol. 6, pp. 48169–48180, 2018.
[13] Z. Liu, C. Yuan, and Y. Zhang, "Active fault-tolerant control of unmanned quadrotor helicopter using linear parameter varying technique," *J. Intell. Robot. Syst.*, vol. 88, nos. 2–4, pp. 415–436, Dec. 2017.
[14] R. C. Avram, X. Zhang, and J. Muse, "Quadrotor actuator fault diagnosis and accommodation using nonlinear adaptive estimators," *IEEE Trans. Control Syst. Technol.*, vol. 25, no. 6, pp. 2219–2226, Nov. 2017.
[15] Y. Wu, K. Hu, X.-M. Sun, and Y. Ma, "Nonlinear control of quadrotor for fault tolerance: A total failure of one actuator," *IEEE Trans. Syst., Man, Cybern. Syst.*, to be published.
[16] T. Avant, U. Lee, B. Katona, and K. Morgansen, "Dynamics, hover configurations, and rotor failure restabilization of a morphing quadrotor," in *Proc. Annu. Amer. Control Conf. (ACC)*, Jun. 2018, pp. 4855–4862.
[17] A.-R. Merheb, H. Noura, and F. Bateman, "Emergency control of AR drone quadrotor UAV suffering a total loss of one rotor," *IEEE/ASME Trans. Mechatronics*, vol. 22, no. 2, pp. 961–971, Apr. 2017.
[18] M. W. Mueller and R. D'Andrea, "Relaxed hover solutions for multicopters: Application to algorithmic redundancy and novel vehicles," *Int. J. Robot. Res.*, vol. 35, no. 8, pp. 873–889, Jul. 2016.
[19] P. Lu and E.-J. Van Kampen, "Active fault-tolerant control for quadrotors subjected to a complete rotor failure," in *Proc. IEEE/RSJ Int. Conf. Intell. Robots Syst. (IROS)*, Sep. 2015, pp. 4698–4703.
[20] A. Lanzon, A. Freddi, and S. Longhi, "Flight control of a quadrotor vehicle subsequent to a rotor failure," *J. Guid., Control, Dyn.*, vol. 37, no. 2, pp. 580–591, Mar. 2014.

[21] V. Lippiello, F. Ruggiero, and D. Serra, "Emergency landing for a quadrotor in case of a propeller failure: A backstepping approach," in *Proc. IEEE/RSJ Int. Conf. Intell. Robots Syst.*, Sep. 2014, pp. 4782–4788.
[22] J. Lan, R. J. Patton, and X. Zhu, "Integrated fault-tolerant control for a 3-DOF helicopter with actuator faults and saturation," *IET Control Theory Appl.*, vol. 11, no. 14, pp. 2232–2241, Sep. 2017.
[23] A. Poultney, C. Kennedy, G. Clayton, and H. Ashrafiuon, "Robust tracking control of quadrotors based on differential flatness: Simulations and experiments," *IEEE/ASME Trans. Mechatronics*, vol. 23, no. 3, pp. 1126–1137, Jun. 2018.
[24] P. Castillo-Garcia, L. E. M. Hernandez, and P. G. Gil, *Indoor Navigation Strategies for Aerial Autonomous Systems*. London, U.K.: Butterworth, 2016.
[25] O. Garcia, P. Ordaz, O.-J. Santos-Sanchez, S. Salazar, and R. Lozano, "Backstepping and robust control for a quadrotor in outdoors environments: An experimental approach," *IEEE Access*, vol. 7, pp. 40636–40648, 2019.
[26] A. Chamseddine, D. Theilliol, Y. Zhang, C. Join, and C. Rabbath, "Active fault-tolerant control system design with trajectory re-planning against actuator faults and saturation: Application to a quadrotor unmanned aerial vehicle," *Int. J. Adapt. Control Signal Process.*, vol. 29, no. 1, pp. 1–23, Jan. 2015.
[27] J. Mohammadpour and C. W. Scherer, *Control of Linear Parameter Varying Systems With Applications*. Springer, 2012.
[28] D. Rotondo, F. Nejjari, and V. Puig, "Robust quasi-LPV model reference FTC of a quadrotor UAV subject to actuator faults," *Int. J. Appl. Math. Comput. Sci.*, vol. 25, no. 1, pp. 7–22, Mar. 2015.
[29] L. Chen, H. Alwi, and C. Edwards, "On the synthesis of an integrated active LPV FTC scheme using sliding modes," *Automatica*, vol. 110, Dec. 2019, Art. no. 108536.
[30] G.-X. Du, Q. Quan, and K.-Y. Cai, "Controllability analysis and degraded control for a class of hexacopters subject to rotor failures," *J. Intell. Robot. Syst.*, vol. 78, no. 1, pp. 143–157, Apr. 2015.
[31] M. Saied, H. Shraim, B. Lussier, I. Fantoni, and C. Francis, "Local controllability and attitude stabilization of multirotor UAVs: Validation on a coaxial octorotor," *Robot. Auto. Syst.*, vol. 91, pp. 128–138, May 2017.
[32] G. Besançon, "Remarks on nonlinear adaptive observer design," *Syst. Control Lett.*, vol. 41, no. 4, pp. 271–280, Nov. 2000.
[33] K. K. Busawon and P. Kabore, "Disturbance attenuation using proportional integral observers," *Int. J. Control*, vol. 74, no. 6, pp. 618–627, Jan. 2001.
[34] H. Ohtake, K. Tanaka, and H. O. Wang, "Fuzzy modeling via sector nonlinearity concept," *Integr. Comput.-Aided Eng.*, vol. 10, no. 4, pp. 333–341, Sep. 2003.
[35] M. Guerrero-Sanchez, H. Abaunza, P. Castillo, R. Lozano, C. Garcia-Beltran, and A. Rodriguez-Palacios, "Passivity-based control for a micro air vehicle using unit quaternions," *Appl. Sci.*, vol. 7, no. 1, p. 13, Dec. 2016.
[36] J. Lofberg, "YALMIP: A toolbox for modeling and optimization in MATLAB," in *Proc. IEEE Int. Conf. Robot. Autom.*, Mar. 2005, pp. 284–289.

**GERARDO ORTIZ-TORRES** received the M.Sc. and Ph.D. degrees in electronic engineering from the National Research and Technological Development Center (CENIDET), in 2014 and 2018, respectively. He is currently a Professor and a Researcher with the University of Guadalajara. His research interests include fault diagnosis, and fault tolerant control systems with applications in unmanned vehicles and process engineering.

**PEDRO CASTILLO** was born in Morelos, Mexico, in January 1975. He received the B.S. degree in electromechanic engineering from the Instituto Tecnologico de Zacatepec, Mexico, in 1997, the M.Sc. degree in electrical engineering from the Centro de Investigación y de Estudios Avanzados (CINVESTAV), Mexico, in 2000, and the Ph.D. degree in automatic control from the University of Technology of Compiègne, France, in 2004. His research topics include real time control applications, nonlinear dynamics and control, aerospace vehicles, vision, and underactuated mechanical systems.

**FELIPE D. J. SORCIA-VÁZQUEZ** was born in Orizaba, Mexico, in 1985. He received the B.S. degree in electronics engineering from the Instituto Tecnológico de Orizaba, Orizaba, Mexico, in 2008, and the M.Sc. degree in electronics engineering and the Dr.Sc. degree from the Centro Nacional de Investigación y Desarrollo Tecnológico (CENIDET), Cuernavaca, Mexico, in 2010 and 2015, respectively.

He is currently a Professor and a Researcher with the University of Guadalajara. His research interests include model predictive control, distributed and decentralized model predictive control, nonlinear control, and real-time control applications.

**JESSE Y. RUMBO-MORALES** received the Ph.D. degree from the Centro Nacional de Investigación y Desarrollo Tecnológico (CENIDET). He is currently a full time Professor of the Centro Universitario de los Valles, Universidad de Guadalajara. He has published national and international journal articles with cites from Scopus. He has graduated 15 bachelor's degree thesis and 15 technical level theses. He has participated in projects, in particular in the construction of a prototype pressure swing adsorption to produce bio-ethanol. Belongs to the SNI. His areas of research are process control, renewable energy, identification of non-linear systems, and automation.

**JORGE A. BRIZUELA-MENDOZA** was born in Guadalajara, Jalisco, Mexico, in 1984. He received the degree in electronics engineering from the Instituto Tecnológico de Cd. Guzmán, Jalisco, Mexico, in 2008, and the master's degrees in mechatronics engineering and the Ph.D. degree in electronics from the Centro Nacional de Investigación y Desarrollo Tecnológico (CENIDET), in 2011 and 2015, respectively. As of 2016, he works at the Centro Universitario de los Valles (CUValles), Universidad de Guadalajara (UDG), as a full-time Professor.

**JAVIER DE LA CRUZ-SOTO** received the master's degree with an emphasis on the operation and control of electric power systems and electricity markets from the Instituto Tecnológico de Morelia and the Ph.D. degree in electrical engineering from CINVESTAV, Guadalajara, where he specialized in the design of small wind turbines. Since 2014, he has been working with INEEL in projects associated with the integration of electric vehicles in distribution networks. He is currently an Electrical Engineer from the Instituto Tecnológico de Sonora. His research areas are energy storage and renewable energy. He is a member of the SNI Level Candidate.

**MARIO MARTÍNEZ-GARCÍA** with academic training in computer engineering in 2001, and received the master's degree in information technology from the University of Guadalajara, Mexico, in 2005, and the Ph.D. degree in research and educational innovation from the University of Malaga, Spain, in 2012, with experience in software development, expert systems, applications for mobile devices, with special interest in research on information technologies applied to education, distributed computing, embedded software, and alternative renewable energy systems.